nanomaterials

MDPI

Type of the Paper (Article)

Förster Resonance Energy Transfer and Enhanced Emission in Cs_4PbBr_6 Nanocrystals Encapsulated in Silicon Nano-Sheets for PeLED Applications

Araceli Herrera Mondragon,[1] Roberto Gonzalez Rodriguez,[1] Noah Hurley,[1] Sinto Varghese,[1] Yan Jiang,[1] Brian Squires,[1] Maoding Cheng, [2] Brooke Davis,[2] Qinglong Jiang,[2] Mansour Mortazavi,[2] Anupama B. Kaul,[3,4] Jeffery L. Coffer, [5] Jingbiao Cui,[1] and Yuankun Lin[1,4,*]

1 Department of Physics, University of North Texas, Denton, TX 76203, USA; araceliherrera-mondragon@my.unt.edu (A. H. M.), Roberto.Gonzalezrodriguez@unt.edu (R. G. D.), NoahHurley@my.unt.edu (N. H.), sintovarghese@my.unt.edu (S. V.), Yan.Jiang@unt.edu (Y. J.), brian.squires@unt.edu (B.S.), Jingbiao.Cui@unt.edu (J. C.)
2Department of Chemistry and Physics, University of Arkansas, Pine Bluff, AR, 71601, USA; chengm@uapb.edu (M. C.), davisb4610@uapb.edu (B.D.), jiangq@uapb.edu (Q.J.), mortazavim@uapb.edu (M.M.)
3Department of Materials Science and Engineering, University of North Texas, Denton, TX 76203, USA; Anupama.Kaul@unt.edu (A.B.K.)
4 Department of Electrical Engineering, University of North Texas, Denton, TX 76203, USA.
5 Department of Chemistry and Biochemistry, Texas Christian University, TCU Box 298860, Fort Worth, TX 76129, USA; j.coffer@tcu.edu (J.L.C.)
* Correspondence: Yuankun.lin@unt.edu; Tel.: +1-940-565-4548

Abstract: Encapsulating Cs_4PbBr_6 quantum dots in silicon nano-sheets not only stabilizes the halide perovskite, but also takes advantage of the nanosheet for a compatible integration with the traditional silicon semiconductor. Here we report the preparation of un-passivated Cs_4PbBr_6 ellipsoidal nanocrystals and pseudo-spherical quantum dots in silicon nano-sheets and their enhanced photoluminescence (PL). For the sample with low concentrations of quantum dots in silicon nano-sheets, the emission from Cs_4PbBr_6 pseudo-spherical quantum dots is quenched and is dominated with Pb^{2+} ion/silicene emission, which is very stable during the whole measurement period. For the high concentration of Cs_4PbBr_6 ellipsoidal nanocrystals in silicon nano-sheets, we have observed Förster resonance energy transfer with up to 87 % efficiency through an oscillation of two PL peaks during on and off of UV excitation, recorded video and PL lifetime measurements. In an area of non-uniform sample containing both ellipsoidal nanocrystals and pseudo-spherical quantum dots where Pb^{2+} ion/silicene emission, broadband emission from quantum dots, bandgap edge emission (515 nm) appear, the 515 nm peak intensity increases 5 times during 30 minutes of UV excitation, probably due to a photon recycling effect. This irradiated sample has been stable for one year of ambient storage. Cs_4PbBr_6 quantum dots encapsulated in silicon nano-sheets can lead to applications of halide perovskite light emitting diodes (PeLEDs) and integration with traditional semiconductor materials.

Keywords: Halide perovskite; Photoluminescence; Cs_4PbBr_6; Förster resonance energy transfer (FRET); fluorescence lifetime image (FLIM); lifetime; enhanced emission; UV exposure; nano-silicon sheets

Citation: To be added by editorial staff during production.

Academic Editor: Firstname Lastname

Received: date
Revised: date
Accepted: date
Published: date

1. Introduction

Solution-processing halide perovskites, such as $APbX_3$ (A=Cs, MA, FA, and PEA (FA, formamidinium; MA, methylammonium; PEA, phenylethylammonium); X = Cl, Br, and I) are very attractive due to their low-cost production and potential commercial application in pure color LED and photovoltaic devices [1–4]. A solar-cell efficiency up to 26.1% has been reported since their discovery [5]. The thermal stability and photo-stability of halide perovskites pose challenges for their commercial applications. Therefore, surface passivation and encapsulation of halide perovskites in nanotubes or polymers is necessary in order to improve their stability [2,6–15]. Sargent and Grätzel's groups have recently applied fluorinated aniliniums for an interfacial passivation for triple cation $Cs_{0.05}MA_{0.05}FA_{0.9}Pb\ (I_{0.95}Br_{0.05})_3$ perovskite films[16]. The accelerating aging tests of halide perovskites under high temperatures and high humidity have reported a power-conversion efficiency of 24.09% and a 1560-hour T85 at maximum power point under 1-sun illumination operating at 85°C and 50% relative humidity [16]. For perovskite light emitting diode (PeLED) applications, the quantum efficiency of bicomponent perovskite nanocomposite can reach near 100% [17] based on the Förster resonance energy transfer (FRET) from the core $CsPbBr_3$ to the shell of $CsPbI_3$. FRET[18,19] has further been reported between $CsPbBr_3$ and $CsPbCl_3$,[20] between $(PEA)_2PbI_4$ and $MAPbBr_3$ [21], and between 2D perovskites.[22]

Cs_4PbBr_6 is a zero-dimensional perovskite that can be easily prepared as quantum dots. Quantum dots of Cs_4PbBr_6 have been stabilized in glass where the photoluminescence (PL) of perovskites has been shifted from 519 to 503 nm. [23] The superior thermal stability[24] and photostability[25] have been reported in $CsPbBr_3$-in-Cs_4PbBr_6 quantum dots. Highly emissive blue (470 nm) quantum dots have resulted in a high photoluminescence quantum yield of >90% in $CsPbBr_3$ + Cs_4PbBr_6 material system [24]. Silicon nano-sheets are 2D layers of silicon with a tunable band gap. $CsPbBr_3$ isolated in silicene has been realized for PeLED applications. [26]. On the other hand, Cs_4PbBr_6 can have a very high photoluminescence quantum yield (PLQY) which can be 2 orders of magnitude higher than its 3D counterpart.[27] Furthermore, it is also desired to stabilize Cs_4PbBr_6 in silicene and use the silicene for integration with traditional semiconductors. FRET can also be incorporated to further improve PLQY for the PeLED application.[17]

In this paper, nanomaterial systems of Cs_4PbBr_6 ellipsoidal nanocrystals and pseudo-spherical quantum dots in silicon nano-sheets have been prepared and their PL emission have been studied. For Cs_4PbBr_6 quantum dots in silicon nano-sheets, a broadband emission has been observed due to the surface trap states of Cs_4PbBr_6. It is replaced by a stable Pb^{2+} ion emission. For the Cs_4PbBr_6 nanocrystals in silicon nano-sheets, we have observed FRET up to 87 % efficiency. A three-month-old sample of Cs_4PbBr_6 nanocrystals in silicon nano-sheets have shown an enhanced emission by 5 times during 30 mins of UV laser irradiation.

2. Materials and Methods

Preparation of Cs_4PbBr_6 nanocrystals: 71.2 mg CsBr and 24.8 mg $PbBr_2$ were dissolved in 0.6 mL DMSO at 80 °C in a vial. The mixture was cooled down slowly while putting it in the methanol chamber. Green Cs_4PbBr_6 crystals are obtained at the bottom of the vial.

Preparation of Cs_4PbBr_6 nanocrystals and quantum dots in silicon nano-sheets: 45 mg of Cs_4PbBr_6 crystals were dissolved in 0.1 mL of DMSO and mixed with a given amount of silicon nano-sheets. In low concentration of Cs_4PbBr_6 in silicon nano-sheets, the prepared Cs_4PbBr_6 solution was diluted by 10 times. The silicon nano-sheets were prepared following the method described in the reference [28]. In brief, the silicon nano-sheets were obtained by removing calcium ions from $CaSi_2$ in concentrated HCl. As examined by TEM, different concentration of the Cs_4PbBr_6 in silicon nano-sheets results in different crystal sizes and shape. Cs_4PbBr_6 crystals in silicon nano-sheets smaller than 10 nm form a pseudo-spherical shape. We call them Cs_4PbBr_6 quantum dots thereafter. Cs_4PbBr_6 crystals in silicon nano-sheets larger than 10 nm form an ellipsoid shape with an elongation in the silicon nano-sheet plane. We call them Cs_4PbBr_6 nanocrystals thereafter.

The material characterizations and crystal structures of Cs_4PbBr_6 crystals, silicon nano-sheets and Cs_4PbBr_6 nanocrystals in silicon nano-sheets were analyzed using Rigaku Miniflex 600 X-ray diffraction (XRD) with CuKα radiation (λ = 0.15405 nm).

Structural characterization was carried out with transmission electron microscopy (TEM) and energy-dispersive X-ray (EDX) in JEOL JEM-2100 at 200 kV. A carbon-coated 200-mesh copper grid was used for the preparation of TEM sample. The solution of Cs_4PbBr_6 nanocrystals in silicon nano-sheets was drop-casted on the copper grid and dried in vacuum.

The PL of Cs_4PbBr_6 crystals and Cs_4PbBr_6 nanocrystals in silicon nano-sheets was excited by the 375 nm UV laser (CrystaLaser). The PL of Cs_4PbBr_6 quantum dots in silicon nano-sheets and pure silicon nano-sheets was excited by He-Cd 325 nm laser (Kimmon). The PL spectra was analyzed by a BaySpec SuperGamut fiber-coupled UV-NIR spectrometer.

Fluorescence lifetime imaging (FLIM), PL decay lines, and lifetime histograms were obtained using a MicroTime 200 time-resolved confocal fluorescence microscope. The measurement was recorded by a PicoQuant PicoHarp 300 time-correlated single-photon-counting. Data acquisition was performed using a software SymPho Time 64. A Picoquant 405 nm picosecond laser was used with a repetition rate of 40 MHz. A cut-off filter of 435 nm was used before the detectors. Neutral density filters were used to reduce the photo counts below 10^6. A 20× objective lens (numerical aperture NA=0.4) was used in the confocal microscope. For the FRET measurements, filters of 490±5 nm (i.e. 485-495 nm) and 530±20 nm (i.e. 510-550 nm) were placed in front of the detectors. The intensity FRET was calculated using thesoftware in the SymPho Time 64.

3. Results

3.1. Material and Structural Characteristics

The prepared solutions of silicon nano-sheets and Cs_4PbBr_6 nanocrystals encapsulated in silicon nano-sheets were drop-casted onto a Si wafer and dried. Figure 1 shows the X-ray diffraction (XRD) of silicon nano-sheet, Cs_4PbBr_6 nanocrystals encapsulated in silicon nano-sheets and bulk Cs_4PbBr_6 crystals. The XRD peaks at 33.1° in Fig. 1a and 1b belong to Si wafer as confirmed in the supporting information in reference[26]. Silicon nano-sheets have XRD peaks at 17.4°, 28.6°, 37.8°, 44.0°, 47.5°, 49.2° and 56.5° (Fig. 1a). [26]. These peaks appear in the XRD of Cs_4PbBr_6 nanocrystals (high concentration) encapsulated in silicon nano-sheets in Fig. 1b, as labeled by yellow squares. The XRD peaks from Cs_4PbBr_6 nanocrystals in Fig. 1b are located at 12.6°, 12.9°, 20.1°, 22.4°, 25.4°, 27.5°, 28.6°, and 30.3°, and are assigned to the low diffraction orders of (012), (110), (113), (300), (024), (131), (214), and (223) planes, respectively. Fig. 1c shows the XRD pattern of bulk Cs_4PbBr_6 for comparison. The XRD pattern in Fig. 1c can be fitted to the hexagonal phase of Cs_4PbBr_6 with a=13.73 Å, b=13.73 Å, c=13.73 Å, α=90.0°, β=90.0°, and γ=120.0° (XRD database Card No.: 1538416). The XRD pattern of Cs_4PbBr_6 quantum dots encapsulated in silicon nano-sheets shows peaks from silicon nano-sheets only due to the low concentration. However, its presence is confirmed by TEM (vide infra).

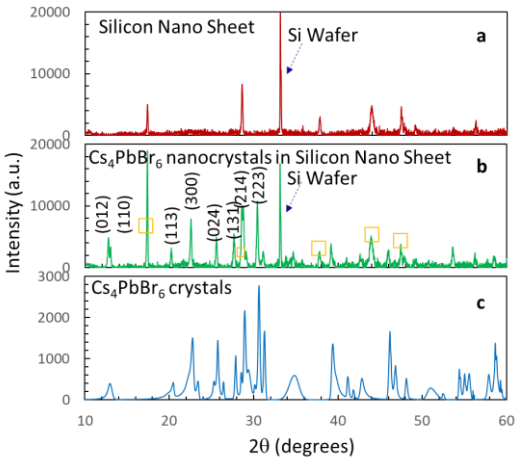

Figure 1. XRD patterns of silicon nano-sheets on Si wafer (a), Cs_4PbBr_6 nanocrystals encapsulated in silicon nano-sheets (b) and bulk Cs_4PbBr_6 (c). The XRD peaks from Si wafer substrate are labelled by dashed arrows. The XRD peaks from silicon nano-sheets are labelled by squares in (b).

Figure 2a shows a zoom-in (enlarged view) of a TEM image of Cs_4PbBr_6 ellipsoida nanocrystals encapsulated in silicon nano-sheets. The dashed arrow in the figure indicates the location of one of Cs_4PbBr_6 nanocrystals (dark regions). All Cs_4PbBr_6 nanocrystals are elongated with the same orientation as indicated by a dashed blue line, assuming in the same plane of a given silicon nano-sheet. From Figure 2a, we can observe that the nanocrystal size is not uniform; the elongated nanocrystals have a larger size in the middle than these at both sides of the elongation. The stretching of the nanocrystals and different sizes along the long nanocrystals will be modeled for the explanation of multiple peaks in PL measurements.

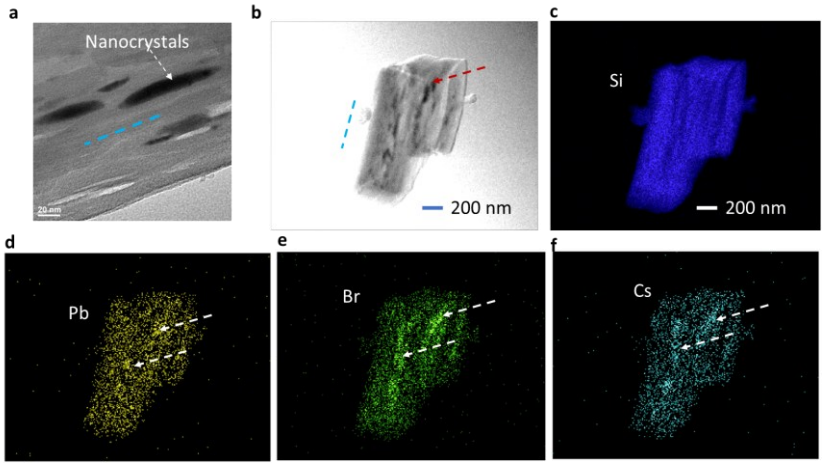

Figure 2: (a) Zoom-in TEM image of Cs_4PbBr_6 nanocrystals encapsulated in silicon nano-sheets; (b) TEM image of one piece of sample of Cs_4PbBr_6 nanocrystals encapsulated in silicon nano-sheets for TEM-EDX. TEM-EDX map of Si (c), Pb (d), Br (e) and Cs (f). Cs_4PbBr_6 nanocrystals are pointed out by dashed arrows in (a) and (b). The same scale bar is used for (b-f). The white arrows in (d, e, f) are for a region with a strong intensity. The dashed lines in (a) and (b) indicate the nano-sheet orientation.

Figure 2b shows a TEM of one piece of sample for TEM-EDX study. The scale bars in (b-f) are the same. The dashed blue line indicates the nano-sheets orientation. One of the dark regions is indicated by an arrow. These nanocrystals in dark regions are in the same orientation. Over 10 of them are revealed on the surface of the TEM. Inside the bulk sample, TEM-EDX maps can reveal more information. The distribution of elements associated with the Cs_4PbBr_6 nanocrystals encapsulated in silicon nano-sheets perovskites (i.e. Si, Pb,

Br, and Cs) is shown in Fig. 2(c, d, e, f), respectively. The elements of Si, Pb, Br, and Cs cover the whole piece of sample in Fig. 2b, as judged by the map shape. It is reasonable that the map intensity of Si in Fig. 2c is uniform due to the role of a host. The map intensity of Pb, Br and Cs is not uniform. Especially in Fig. 2e, it is very clear to see that the strong intensity regions (indicated by dashed white arrows for example) correspond to the dark regions in Fig. 2b.

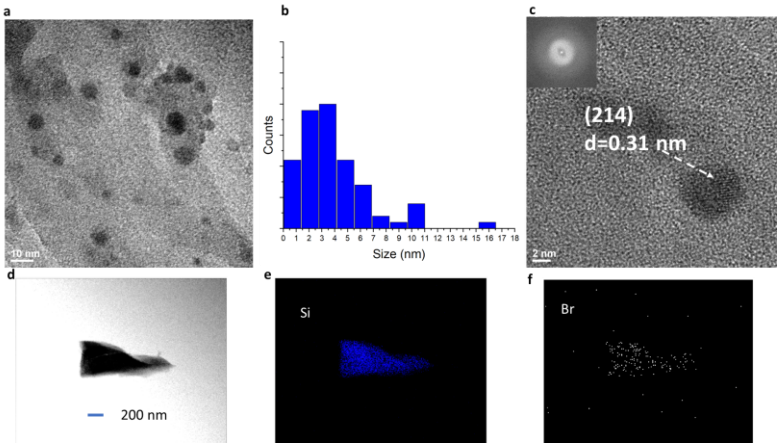

Figure 3: (a) TEM image of Cs_4PbBr_6 quantum dots encapsulated in silicon nano-sheets; (b) Size distribution of Cs_4PbBr_6 quantum dots encapsulated in silicon nano-sheets. (c) High resolution TEM (HRTEM) of Cs_4PbBr_6 quantum dots and the corresponding FFT. TEM of one piece of the sample (d) and its TEM-EDX map of Si (e) and Br (f). The same scale bar is used for (d-f).

Diffraction peaks from Cs_4PbBr_6 quantum dots did not show up in XRD pattern due to their low concentration (diluted by 10 times). TEM was able to observe the quantum dots. Figure 3a shows a typical TEM image of Cs_4PbBr_6 pseudo-spherical quantum dots encapsulated in silicon nano-sheets. The size of quantum dots is not uniform. Figure 3b shows the size distribution of quantum dots in a range of 1 to 16 nm. The mean size is 4.67 nm. Figure 3c shows high-resolution TEM (HRTEM) of quantum dots and fast Fourier transform (FFT) patterns. A d-value of 0.31 nm was obtained, corresponding to the space between (214) plane of hexagonal Cs_4PbBr_6. Figure 3d shows a TEM image of one piece of the sample and its distribution of elements associated with the Cs_4PbBr_6 quantum dots encapsulated in silicon nano-sheets perovskites in Fig. 3(e, f) for Si and Br as an example, respectively. The elements of Si cover the whole sample in Fig. 3e while the map intensity of Br is not as dense as Si due to the low concentration of quantum dots.

3.2. PL spectra and Förster resonance energy transfer

Firstly, we measured the absorption of bulk Cs_4PbBr_6, Cs_4PbBr_6 nanocrystals and quantum dots in DMSO solution before they were mixed with silicon nano-sheets, where narrow peaks were observed at 295, 287 and 272 nm, respectively. We then measured PL for bulk Cs_4PbBr_6, its ellipsoidal nanocrystals and pseudo-spherical quantum dots encapsulated in silicon nano-sheets. Fig. 4b shows normalized PLs with a peak position at 520 nm for bulk Cs_4PbBr_6, two peaks at 512 and 490 nm for Cs_4PbBr_6 nanocrystals and a broad peak centered at 480 nm for Cs_4PbBr_6 quantum dots. With a small crystal size, the PL peak is blue shifted, similar to what has been observed in $CsPbBr_3$ in silicene and bulk $CsPbBr_3$. The broad peak of Cs_4PbBr_6 quantum dots in Fig. 4b can be due to the un-passivated surfaces and its surface state. Similar to other results[29], Cs_4PbBr_6 had a very small spectral overlap of absorption and PL emission with Stokes shift up to 1.82 eV. Defect states due to Br-poor vacancy or local deformation of $[PbBr_6]^{4-}$ octahedra were used to explain the large Stokes shift. [29–32] Although a shift of narrow peak with the crystal size has been observed in Fig. 4a, such a large Stokes shift poses a complexity in explaining the FRET below in Cs_4PbBr_6 in silicon nano-sheets.

The PL in Fig. 4b for Cs_4PbBr_6 nanocrystals in silicon nano-sheets was measured after several minutes of UV exposure. In the short period of UV 375 nm laser exposure, the peak at 512 nm is very weak initially, then increases its intensity from 0 to 28 seconds, and finally its intensity is higher than the peak at 490 nm, as shown in Fig. 4c. We also recorded a Video S1 "PL peak intensity oscillation". We can see the increase of peak intensity at 512 nm, turning off the UV laser during the 36-42 seconds, dropping of peak intensity, and increasing again after the UV laser is on. Figure 4d shows the peak intensity as a function of UV exposure times where we see an increase in intensity by more than 2 times for 512 nm emission in 20 seconds.

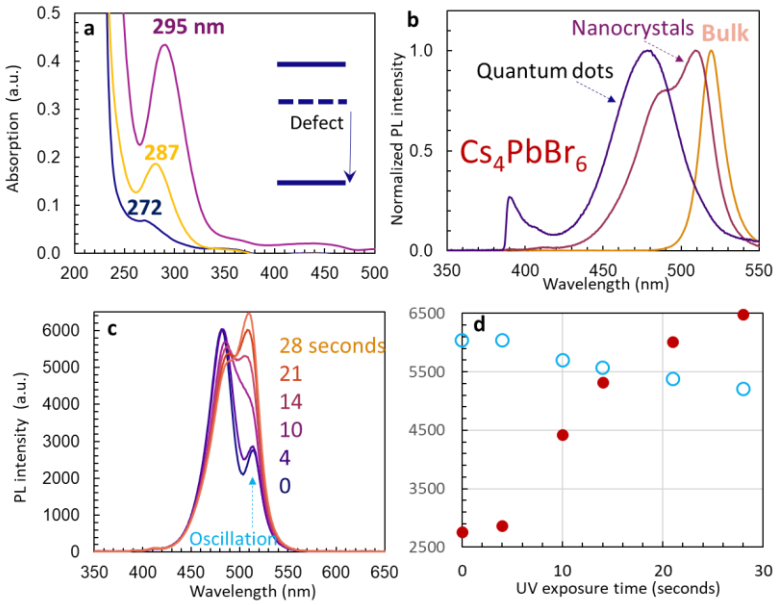

Figure 4: (a) Absorption of bulk Cs_4PbBr_6 (pink line), Cs_4PbBr_6 nanocrystals (yellow line) and quantum dots (blue line) in DMSO solution. (b) Normalized PL spectra of bulk Cs_4PbBr_6 (yellow line), Cs_4PbBr_6 nanocrystals (pink line) and quantum dots (blue line) encapsulated in silicon nano-sheets. (c) PL spectra of Cs_4PbBr_6 nanocrystals encapsulated in silicon nano-sheets at 0, 4, 10, 14, 21 and 28 seconds after UV excitation laser is turned on. (d) PL intensity at two wavelength (512 nm in red and 490 nm in blue) as a function of UV exposure time.

In order to understand both the intensity oscillation of the 512 nm emission peak and exchange of peak intensity of both PL lines in Cs_4PbBr_6 nanocrystals encapsulated in silicon nano-sheets, we measured the lifetime of PL peaks and FRET in the next steps. Due to intensity change and shift of PL peak with UV laser exposure time, we measured the PL after the UV laser had been turned on for several minutes (typical time for PL lifetime imaging). We measured PL for 6 times of the irradiation hardening starting from yellow to dark blue as shown in Fig. 5a. The irradiation hardened Cs_4PbBr_6 nanocrystals have PL peaks at 490 and 512 nm. We used bandpass filters of 490±5 nm (i.e. 485-495 nm) and 530±20 nm (i.e. 510-550 nm) and measured FLIM. After fitting and calculation, Fig. 5b and 5c show the average lifetime histogram for PL peak at 490 and 512 nm, respectively. The lifetime events were controlled below 10^6 for measurement accuracy. As seen from Fig. 5b and 5c, the average lifetime is centered at 6.8 ns for 490 nm and 5.0 ns for 512 nm. Their PL decay lines are shown Fig. 5d. As nanocrystal size becomes smaller, PL peak usually blueshifts [33]. The PL of 490 nm comes from a smaller nanocrystal than that for 512 nm. The more surface localized charges [34] (also more surface trap states) in smaller nanocrystals increase the PL lifetime and also make the lifetime histogram curve broader in Fig. 5b than that in Fig. 5c.

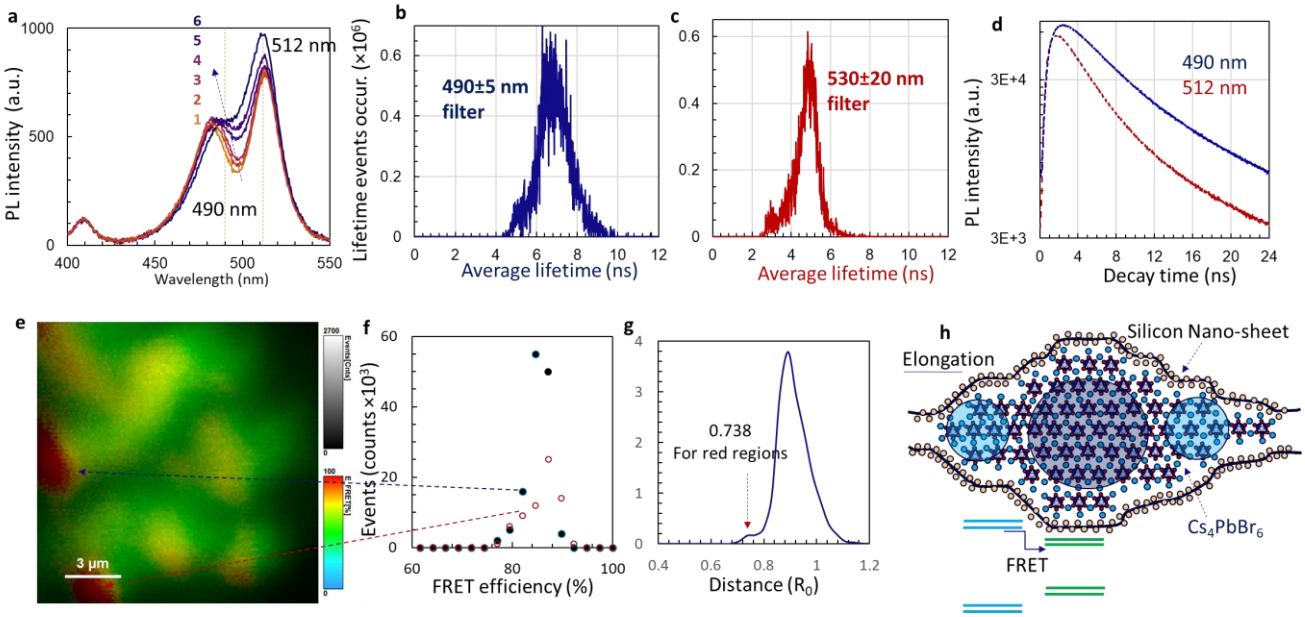

Figure 5: (a) PL spectra measured after Cs_4PbBr_6 nanocrystals encapsulated in silicon nano-sheets have been exposed to UV 375 nm laser for several minutes. Six of them have been measured starting with "1" and ending with "6". (b-c) Average PL lifetime histogram measured with bandpass filters of 490±5 nm (i.e. 485-495 nm) (b) and 530±20 nm (c). (d) PL intensity decay curves for 490 and 512 nm. (e) Intensity and efficiency of FRET and (f) the FRET efficiency histogram for two red regions in (d) as indicated by dashed arrows. (g) Occurred FRET events at different distances. (h) Schematic of elongated Cs_4PbBr_6 nanocrystals encapsulated in silicon nano-sheets. The circles are for eye guidance of different crystal sizes. The different sizes lead to different bandgaps for FRET.

Using bandpass filters of 490±5 nm and 530±20 nm, we measured FLIM and calculated FRET events and efficiency between 490 nm and 512 nm as shown in Fig. 5e. The FRET efficiency E[19] is defined in Eq. 1:

$$E = \frac{1}{\left(\frac{R}{R_0}\right)^6 + 1} \qquad (1)$$

Where Ro is the distance between Cs_4PbBr_6 donor (490 nm emission) and Cs_4PbBr_6 acceptor (512 nm emission) with FRET efficiency of 50 %, and R is the distance between the donor and acceptor. Non-uniformity in FRET efficiency is clearly observed. Based on the scale bar, most of areas are covered by a green color with approximately 66 % efficiency with a distance of $0.89R_o$ as also calculated by Eq. (1). For the two red regions, we processed with "region of interest" and obtained a FRET efficiency histogram in Fig. 5f. Both red regions have a FRET efficiency of 86-87%, corresponding to a distance of $0.738\ R_o$ as indicated by the red arrow in Fig. 5g, where the occurred FRET events over the map region is plotted with respect to R. Fig. 5h shows a schematic of proposed model of Cs_4PbBr_6 nanocrystals encapsulated in silicon nano-sheets with an elongation in horizontal direction, following the information that was obtained in TEM in Fig. 2a and 2b for Cs_4PbBr_6 ellipsoidal nanocrystals in dark regions. The circles in Fig. 5h for eye guidance only. We have a schematic of wide (blue lines) and narrow (green lines) bandgaps for Cs_4PbBr_6 nanocrystals above. FRET can occur between these wide and narrow bandgaps.

3.3. Stability of un-passivated Cs_4PbBr_6 and enhanced PL emissions

We present the stability of un-passivated Cs_4PbBr_6 quantum dots encapsulated in silicon nano-sheets, non-uniformity, Pb^{2+} ion emission and enhancement of 512 nm emission. Figure 6a shows PL spectra of Cs_4PbBr_6 quantum dots encapsulated in silicon nano-sheets

after continuous UV laser exposure of 0, 1, 2, 3, 4, 5, 10, 25, and 90 minutes. The broad peak centered at 483 nm drops in intensity very quickly within 5 seconds. The intensity of Pb^{2+} ion emission [31,32] at 410 nm increases quickly with increasing exposure. Fig. 6b shows the PL intensities as a function of UV laser exposure times for these two peaks. At 12 minutes, the intensity of 483 nm peaks reaches almost zero while the Pb^{2+} ion emission reached the maximum at 12 minutes and is stable up to the end of measurement (90 minutes), indicating that un-passivated Cs_4PbBr_6 quantum dots are not stable and isolated Pb^{2+} ion is formed and stable. After longer UV exposure time, Pb^{2+} ion emission becomes stronger. Fig. 6c shows PL of Pb^{2+} ion emission after UV degradation of Cs_4PbBr_6 quantum dots for 5 hrs. The peak below 400 nm is emission tail of 375 nm laser after a band cutoff filter. To confirm that, we excited the PL of degraded Cs_4PbBr_6 quantum dots by UV 325 nm laser. Fig. 6d shows PL of degraded Cs_4PbBr_6 quantum dots with one peak only at 410 nm. We also show PL spectrum of pure silicene, excited by UV 325 nm laser for a comparison. The silicene (silicon nano-sheets) has no PL between 350-550 nm.

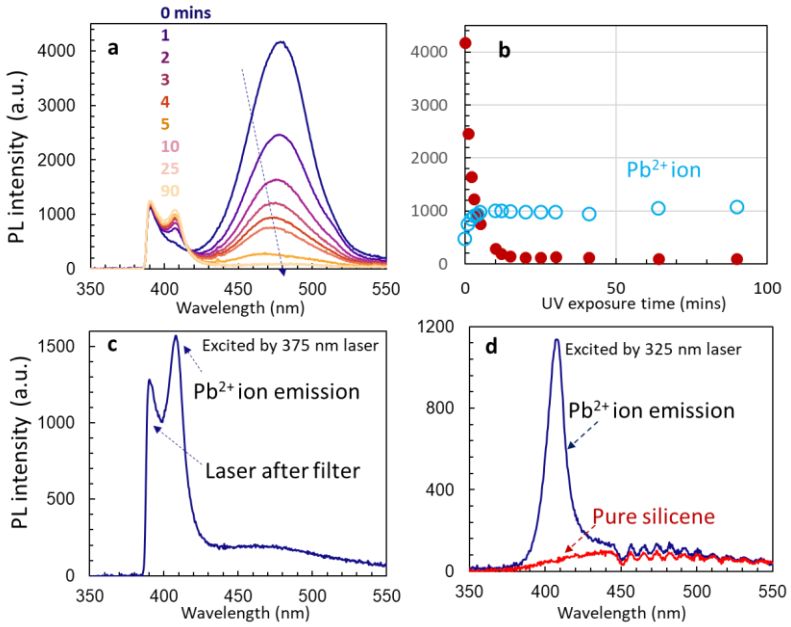

Figure 6: (a) PL spectra of Cs_4PbBr_6 quantum dots encapsulated in silicon nano-sheets after different times of UV laser exposure of 0, 1, 2, 3, 4, 5, 10, 25, and 90 minutes; (b) PL intensities as a function of UV laser exposure times for 483 nm (red circles) and Pb^{2+} ion emission at 410 nm; (c) PL of Pb^{2+} ion emission after UV degradation of Cs_4PbBr_6 quantum dots for 5 hrs. (d) PL of degraded Cs_4PbBr_6 quantum dots and pure silicene, excited by UV 325 nm laser.

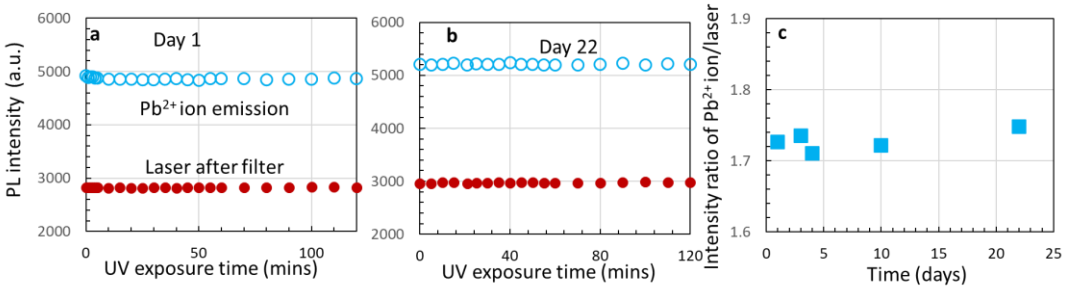

Figure 7: PL intensity of Pb^{2+} ion emission and laser tail intensity after a filter on day 1 (a), day 22 (b). The laser intensity is stable and used as a reference for intensity ratio of Pb^{2+} ion emission at different days (c).

We further studied the stability of Pb^{2+} ion emission. We picked up a degraded Cs_4PbBr_6 quantum dots and monitored the intensity stability of 410 nm peak (Pb^{2+} ion emission [31,32]) as shown in Figure 7a on day-1. The red circles in the figure indicate that the laser power is very stable. The intensity of Pb^{2+} ion emission changed slightly at the very beginning then stable. We measured the intensity of Pb^{2+} ion emission on day-3, 4, 10 and 22 for 2 hours. Figure 7b plots the intensity of Pb^{2+} ion emission on day-22 as a representative example and Figure 7c shows the intensity ratio of Pb^{2+} ion emission over the laser tail power. Overall, the intrinsic Pb^{2+} ion emission is stable.

With above understanding of stability of Pb^{2+} ions and instability of Cs_4PbBr_6 quantum dots, we further studied a region of sample where Cs_4PbBr_6 nanocrystals have three PL peaks at 515 nm, 475 nm and 410 nm as shown in Figure 8a. The shift of 490 nm in Fig. 5a to 475 nm in Fig. 8a indicates smaller nanocrystal sizes in Fig. 8a than that in Fig. 5a. From both Fig. 8a and 8b, we can learn that the intensity of PL peak 515 nm is initially weaker than 475 nm, increases at the very beginning of UV 375 nm exposure, becomes stronger than 475 nm, then decreases in intensity with increasing exposure times. For 475 nm, its intensity drops quickly at the very beginning of UV exposure and drops at a slower slope together with 515 nm in Fig. 8b. The dropping of intensity of both PL peaks can be caused by the instability of Cs_4PbBr_6 nanocrystals related to 475 nm.

We waited for 3 months for the disappearance of 475 nm. As shown in Fig. 8c, the 3-month-old sample has a weak peak at 460 nm. However, the Pb^{2+} ion emission becomes relatively strong due to the degradation of Cs_4PbBr_6 nanocrystals. In such an aged sample, the intensity of PL 515 nm increases 5 times upon exposing the sample to UV 375 nm laser for 15 minutes and reaches the maximum after 30 minutes as shown in both Fig. 8c and 8d. The Pb^{2+} ion emission at 417 nm was stable and the intensity of 460 nm varied slightly. The stable PL of Pb^{2+} ion emission can lead to a possibility of photon recycling (the process of photon re-absorption and internal re-emission from Pb^{2+} to 515 nm) for the enhancement of 515 nm. Future research can be performed on the passivation of Cs_4PbBr_6 nanocrystals then further encapsulated in silicon nano-sheets for photoelectric devices.

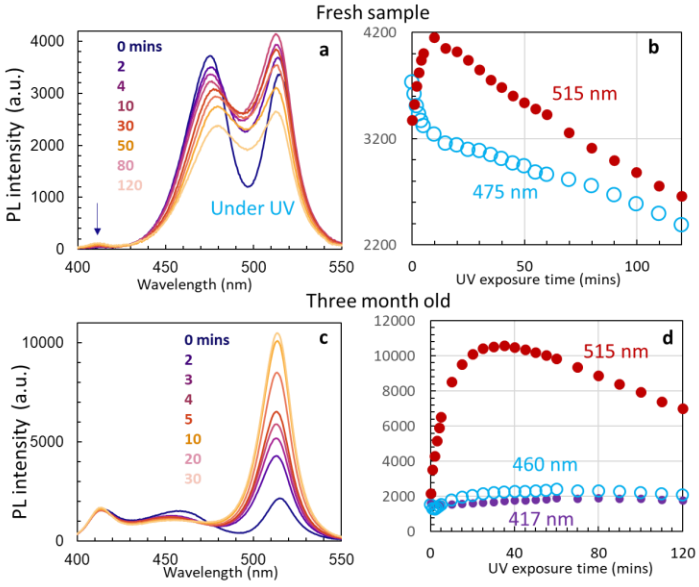

Figure 8: (a) PL spectra in a region of sample where Cs_4PbBr_6 nanocrystals have three PL peaks at 515 nm, 475 nm and weak 410 nm line (as indicated by an arrow) after 0, 2, 4, 10, 30, 50 80, and 120 minutes of UV 375 nm laser exposure; (b) PL intensities of 515 nm and 475 nm as a function of times of UV 375 nm laser exposure. (c) PL spectra from 3-month-old sample after 0, 2, 3, 4, 5, 10, 20, and 30 minutes of UV 375 nm laser exposure; (d) PL intensities of 515 nm, 460 nm, and 417 nm as a function of times of UV 375 nm laser exposure.

After 12 months of ambient storage of Cs_4PbBr_6 nanocrystals in silicon nano-sheets, we were still able to observe the FRET as shown in Fig. 9. This time, the peak intensity at 487 nm is stable during the measurement period from 0 to 120 mins. The peak intensity at 515 nm is stronger than 487 nm peak. Its intensity increased from 6400 to 7600 in a short time, then stays almost constant. By comparison of two peak intensities in Fig. 9a and 9b, we can see that FRET plays a crucial role in PL enhancement of 515 nm for PeLED applications.

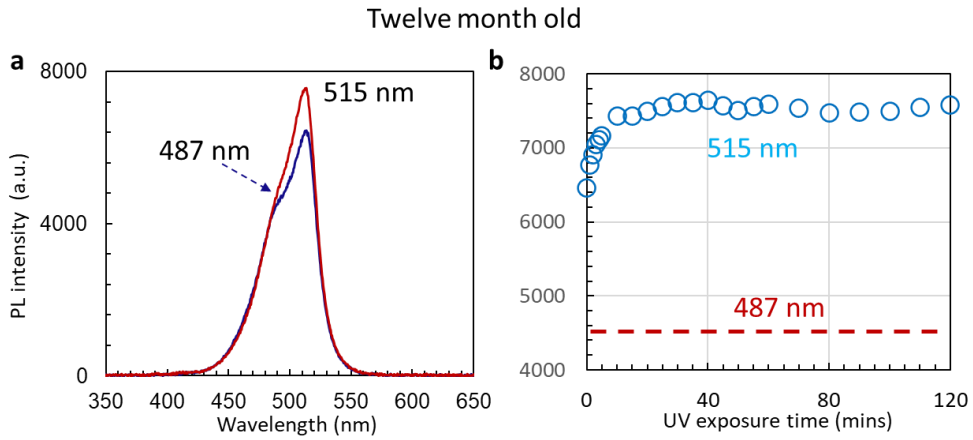

Figure 9: (a) PL spectra of 12-month old sample of Cs_4PbBr_6 nanocrystals encapsulated in silicon nano-sheets at 0 (blue line) and 120 minutes (red line) after UV excitation laser is turned on. (b) PL intensity at 515 nm as a function of UV exposure time. We did not conduct the fitting of peak intensity for 487 nm. The dashed red line is for eye-guidance only.

4. Discussion

Cs_4PbBr_6 was reported to be stable under alpha-particle excitation.[35] We first discuss the UV irradiation effect on Cs_4PbBr_6 nanocrystals encapsulated in silicon nano-sheets. After 12 months, we rechecked XRD for the sample as shown in Fig. 10. As we can see from the figure, XRD peaks from silicon nano-sheet were still observed, indicating silicon nano-sheets were stable in 12 months. We can still observe the XRD peaks from Cs_4PbBr_6 nanocrystals at 12.6°, 12.9°, 22.4°, 25.4°, 27.5°, 28.6°, and 30.3° due to low diffraction orders of (012), (110), (300), (024), (131), (214), and (223) planes, respectively. Diffraction from the (113) plane is missing and XRD peaks are weaker from the aged sample than the fresh one, corresponding to the fact that the broad peak around 460 nm from the Cs_4PbBr_6 became weak and Pb^{2+} emission appeared after UV irradiation in Fig. 6 and Fig. 8.

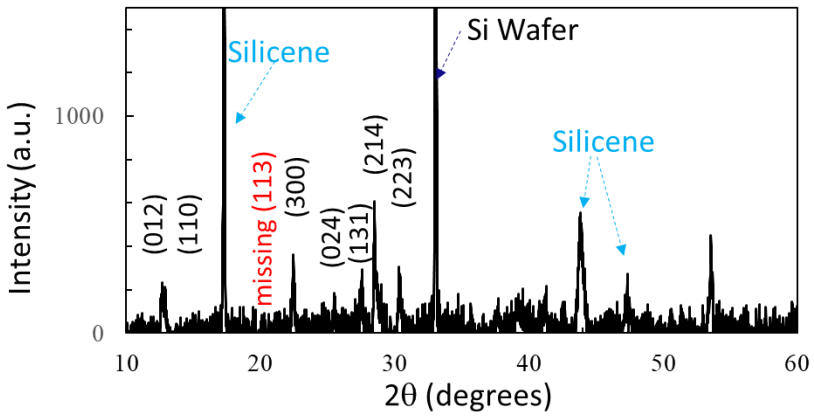

Figure 10. XRD patterns of Cs_4PbBr_6 nanocrystals encapsulated in silicon nano-sheets that are 12-month old.

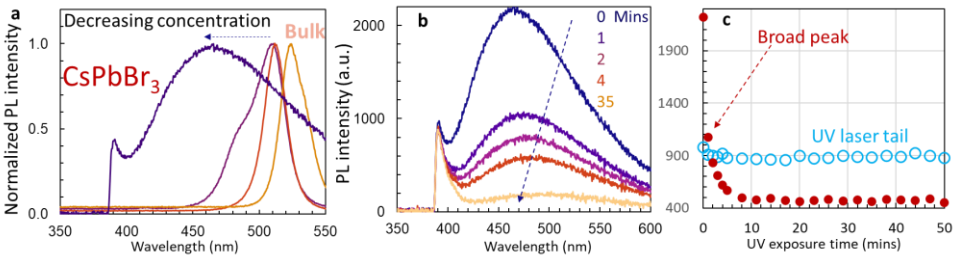

Figure 11: (a) Normalized PL spectra of $CsPbBr_3$ with decreasing concentration in silicon nano-sheet. (b) PL spectra of $CsPbBr_3$ quantum dots encapsulated in silicon nano-sheets after different times of UV laser exposure of 0, 1, 2, 4, and 35 minutes; (c) PL intensities as a function of UV laser exposure times for broad peak centered at 466 nm.

We further discuss why the PL peak from Cs_4PbBr_6 quantum dots is broader than those from nano crystal or bulk material. Usually PL peak becomes narrower when the nanocrystal size becomes smaller due to the quantum discrete state. [33] We assume that there are many surface trap states in the interface of silicon nano-sheets and un-passivated quantum dots, leading to a broad PL peak. To confirm the assumption, we compare our results from Cs_4PbBr_6 with those from $CsPbBr_3$. We prepared $CsPbBr_3$ encapsulated in silicon nano-sheets with decreasing concentration (the quantity of concentration was ignored) and measured their PL in Fig. 11a. Similarly, a broad peak was observed at the low concentration of $CsPbBr_3$ in silicon nano-sheets. The intensity of the broad peak dropped quickly during the UV 375 nm laser irradiation as shown in Fig. 11b and 11c. The only difference between the Cs_4PbBr_6 and $CsPbBr_3$ samples is that there is no Pb^{2+} ion emission in $CsPbBr_3$ sample.

5. Conclusions

Silicon nano-sheets have been used to encapsulate Cs_4PbBr_6 nanocrystals for potential integration with traditional semiconductors. For low concentration of un-passivated Cs_4PbBr_6 in silicon nano-sheets, pseudo-spherical quantum dots have been formed with a broad PL peak which is not stable upon an irradiation with a UV 375 nm laser. The Pb^{2+} ion emission has been stable upon the degradation of Cs_4PbBr_6 quantum dots. For high concentrations of un-passivated Cs_4PbBr_6 in silicon nano-sheets, ellipsoidal nanocrystals have been observed. Intensity oscillation of two PL peaks have been observed upon UV laser on and off and explained by FRET with an efficiency up to 86-87%. In a sample with three PL peaks at 515, 475 and 410 nm, the degraded (aged for 3 months) sample has shown stable Pb^{2+} ion/silicene emission, and enhanced intensity by 5 times for 515 nm, presumably due to photon recycling from Pb^{2+} ion/silicene emission to 515 nm.

Supplementary Materials: The following supporting information can be downloaded at: www.mdpi.com/xxx/s1, Video S1: PL peak intensity oscillation.

Author Contributions: Conceptualization, Y.L., J.C. and R.G.R.; methodology, G.G.R., Y.L., A.H.M. and J.C.; software, N.H., A.H.M. and S.V.; formal analysis, A.H.M., R.G.R. and Y.L.; investigation, A.H.M., R.G.R., N.H., B.S. and S.V.; resources, J.L.C., B.S., J.C. and Y.L.; Material synthesis, B. D., M. C., Q.J. and R.G.R; writing—original draft preparation, A.H.M., R.G.R, Q.J. and Y.L.; writing—review and editing, all; visualization, Y.L. and Y.J.; supervision, Q.J., A.B.K., M.M., J.L.C., J.C. and Y.L.; funding acquisition, Q.J., A.B.K., M.M., J.C. and Y.L.; Y.Y. All authors have read and agreed to the published version of the manuscript.

Funding: This research was partially supported by the U.S. National Science Foundation, grant number 2128367, grant number 2228891 and by the Department of Energy/National Nuclear Security Administration under Award Number DE-NA0004114.

Data Availability Statement: Data will be available upon request.

Conflicts of Interest: The authors declare no conflict of interest. This report was prepared as an account of work sponsored by an agency of the United States Government. Neither the United States Government nor any agency thereof, nor any of their employees, makes any warranty, express or implied, or assumes any legal liability or responsibility for the accuracy, completeness, or usefulness of any information, apparatus, product, or process disclosed, or represents that its use would not infringe privately owned rights. Reference herein to any specific commercial product, process, or service by trade name, trademark, manufacturer, or otherwise does not necessarily constitute or imply its endorsement, recommendation, or favoring by the United States Government or any agency thereof. The views and opinions of authors expressed herein do not necessarily state or reflect those of the United States Government or any agency thereof.

References

1. Xing, G.; Mathews, N.; Lim, S.S.; Yantara, N.; Liu, X.; Sabba, D.; Grätzel, M.; Mhaisalkar, S.; Sum, T.C. Low-Temperature Solution-Processed Wavelength-Tunable Perovskites for Lasing. *Nat Mater* **2014**, *13*, 476–480, doi:10.1038/nmat3911.
2. Tan, H.; Jain, A.; Voznyy, O.; Lan, X.; García de Arquer, F.P.; Fan, J.Z.; Quintero-Bermudez, R.; Yuan, M.; Zhang, B.; Zhao, Y.; et al. Efficient and Stable Solution-Processed Planar Perovskite Solar Cells via Contact Passivation. *Science (1979)* **2017**, *355*, 722–726, doi:10.1126/science.aai9081.
3. Nie, W.; Tsai, H.; Asadpour, R.; Blancon, J.-C.; Neukirch, A.J.; Gupta, G.; Crochet, J.J.; Chhowalla, M.; Tretiak, S.; Alam, M.A.; et al. High-Efficiency Solution-Processed Perovskite Solar Cells with Millimeter-Scale Grains. *Science (1979)* **2015**, *347*, 522–525, doi:10.1126/science.aaa0472.
4. Zhang, L.; Hu, S.; Guo, M.; Ren, Y.; Wei, L.; Li, W.; Lin, F.; Yang, Z.; Yang, Z.; Liu, C.; et al. Manipulation of Charge Dynamics for Efficient and Bright Blue Perovskite Light-Emitting Diodes with Chiral Ligands. *Advanced Materials* **2023**, *35*, 2302059, doi:10.1002/adma.202302059.
5. Finkenauer, B.P.; Akriti; Ma, K.; Dou, L. Degradation and Self-Healing in Perovskite Solar Cells. *ACS Appl Mater Interfaces* **2022**, *14*, 24073–24088, doi:10.1021/acsami.2c01925.
6. Jiao, H.; Ni, Z.; Shi, Z.; Fei, C.; Liu, Y.; Dai, X.; Huang, J. Perovskite Grain Wrapping by Converting Interfaces and Grain Boundaries into Robust and Water-Insoluble Low-Dimensional Perovskites. *Sci Adv* **2022**, *8*, abq4524, doi:10.1126/sciadv.abq4524.
7. Chen, S.; Dai, X.; Xu, S.; Jiao, H.; Zhao, L.; Huang, J. Stabilizing Perovskite-Substrate Interfaces for High-Performance Perovskite Modules. *Science (1979)* **2021**, *373*, 902–907, doi:10.1126/science.abi6323.
8. Gonzalez-Rodriguez, R.; Hathaway, E.; Lin, Y.; Coffer, J.L.; Cui, J. Encapsulated MAPbBr $_3$ in Nickel Oxide Nanotubes and Their Electroluminescence. *Nanoscale* **2022**, *14*, 6417–6424, doi:10.1039/D2NR00019A.
9. Abdi-Jalebi, M.; Andaji-Garmaroudi, Z.; Cacovich, S.; Stavrakas, C.; Philippe, B.; Richter, J.M.; Alsari, M.; Booker, E.P.; Hutter, E.M.; Pearson, A.J.; et al. Maximizing and Stabilizing Luminescence from Halide Perovskites with Potassium Passivation. *Nature* **2018**, *555*, 497–501, doi:10.1038/nature25989.
10. Xiong, S.; Hou, Z.; Zou, S.; Lu, X.; Yang, J.; Hao, T.; Zhou, Z.; Xu, J.; Zeng, Y.; Xiao, W.; et al. Direct Observation on P- to n-Type Transformation of Perovskite Surface Region during Defect Passivation Driving High Photovoltaic Efficiency. *Joule* **2021**, *5*, 467–480, doi:10.1016/j.joule.2020.12.009.
11. Fang, H.-H.; Yang, J.; Tao, S.; Adjokatse, S.; Kamminga, M.E.; Ye, J.; Blake, G.R.; Even, J.; Loi, M.A. Unravelling Light-Induced Degradation of Layered Perovskite Crystals and Design of Efficient Encapsulation for Improved Photostability. *Adv Funct Mater* **2018**, *28*, 1800305, doi:10.1002/adfm.201800305.
12. Raja, S.N.; Bekenstein, Y.; Koc, M.A.; Fischer, S.; Zhang, D.; Lin, L.; Ritchie, R.O.; Yang, P.; Alivisatos, A.P. Encapsulation of Perovskite Nanocrystals into Macroscale Polymer Matrices: Enhanced Stability and

Polarization. *ACS Appl Mater Interfaces* **2016**, *8*, 35523–35533, doi:10.1021/ACSAMI.6B09443/SUPPL_FILE/AM6B09443_SI_001.PDF.

13. Konidakis, I.; Karagiannaki, A.; Stratakis, E. Advanced Composite Glasses with Metallic, Perovskite, and Two-Dimensional Nanocrystals for Optoelectronic and Photonic Applications. *Nanoscale* **2022**, *14*, 2966–2989, doi:10.1039/D1NR07711B.
14. He, H.; Cui, Y.; Li, B.; Wang, B.; Jin, C.; Yu, J.; Yao, L.; Yang, Y.; Chen, B.; Qian, G. Confinement of Perovskite-QDs within a Single MOF Crystal for Significantly Enhanced Multiphoton Excited Luminescence. *Advanced Materials* **2019**, *31*, 1806897, doi:10.1002/adma.201806897.
15. Lin, Y.; Fan, X.; Yang, X.; Zheng, X.; Huang, W.; Shangguan, Z.; Wang, Y.; Kuo, H.; Wu, T.; Chen, Z. Remarkable Black-Phase Robustness of $CsPbI_3$ Nanocrystals Sealed in Solid SiO_2/AlO_x Sub-Micron Particles. *Small* **2021**, *17*, 2103510, doi:10.1002/smll.202103510.
16. Park, S.M.; Wei, M.; Xu, J.; Atapattu, H.R.; Eickemeyer, F.T.; Darabi, K.; Grater, L.; Yang, Y.; Liu, C.; Teale, S.; et al. Engineering Ligand Reactivity Enables High-Temperature Operation of Stable Perovskite Solar Cells. *Science (1979)* **2023**, *381*, 209–215, doi:10.1126/science.adi4107.
17. Fan, X.; Wang, S.; Yang, X.; Zhong, C.; Chen, G.; Yu, C.; Chen, Y.; Wu, T.; Kuo, H.; Lin, Y.; et al. Brightened Bicomponent Perovskite Nanocomposite Based on Förster Resonance Energy Transfer for Micro-LED Displays. *Advanced Materials* **2023**, *35*, 2300834, doi:10.1002/adma.202300834.
18. Rabouw, F.T.; den Hartog, S.A.; Senden, T.; Meijerink, A. Photonic Effects on the Förster Resonance Energy Transfer Efficiency. *Nat Commun* **2014**, *5*, 3610, doi:10.1038/ncomms4610.
19. Zhang, B.; Lyu, G.; Kelly, E.A.; Evans, R.C. Förster Resonance Energy Transfer in Luminescent Solar Concentrators. *Advanced Science* **2022**, *9*, doi:10.1002/advs.202201160.
20. Mishra, L.; Behera, R.K.; Panigrahi, A.; Sarangi, M.K. Förster Resonance Energy Transfer Assisted Enhancement in Optoelectronic Properties of Metal Halide Perovskite Nanocrystals. *J Phys Chem Lett* **2022**, *13*, 4357–4364, doi:10.1021/acs.jpclett.2c00764.
21. Song, Y.; Zhang, C.; Liu, W.; Li, X.; Long, H.; Wang, K.; Wang, B.; Lu, P. High-Efficiency Energy Transfer in Perovskite Heterostructures. *Opt Express* **2018**, *26*, 18448, doi:10.1364/OE.26.018448.
22. Panuganti, S.; Besteiro, L. V.; Vasileiadou, E.S.; Hoffman, J.M.; Govorov, A.O.; Gray, S.K.; Kanatzidis, M.G.; Schaller, R.D. Distance Dependence of Förster Resonance Energy Transfer Rates in 2D Perovskite Quantum Wells via Control of Organic Spacer Length. *J Am Chem Soc* **2021**, *143*, 4244–4252, doi:10.1021/jacs.0c12441.
23. Li, S.; Liu, G.; Liu, Q.; Nie, L.; Yao, G.; Zeng, F.; He, Y.; Xiang, W. Ultrastable Zero-Dimensional Cs_4PbBr_6 Perovskite Quantum Dot Glass. *ACS Sustain Chem Eng* **2020**, *8*, acssuschemeng.0c03914, doi:10.1021/acssuschemeng.0c03914.
24. Kim, H.; Park, J.H.; Kim, K.; Lee, D.; Song, M.H.; Park, J. Highly Emissive Blue Quantum Dots with Superior Thermal Stability via In Situ Surface Reconstruction of Mixed $CsPbBr_3$ –Cs_4PbBr_6 Nanocrystals. *Advanced Science* **2022**, *9*, doi:10.1002/advs.202104660.
25. Leitão, M.F.; Islim, M.S.; Yin, L.; Viola, S.; Watson, S.; Kelly, A.; Dong, Y.; Li, X.; Zeng, H.; Videv, S.; et al. Pump-Power-Dependence of a $CsPbBr_3$-in-Cs_4PbBr_6 Quantum Dot Color Converter. *Opt Mater Express* **2019**, *9*, 3504, doi:10.1364/OME.9.003504.
26. Gonzalez-Rodriguez, R.; Hathaway, E.; Paulette, H.; Coffer, J.L.; Lin, Y.; Cui, J. Two-Dimensional Quantum-Confined CsPbBr3 in Silicene for LED Applications. *ACS Appl Nano Mater* **2023**, *6*, 4028–4033.

27. Saidaminov, M.I.; Almutlaq, J.; Sarmah, S.; Dursun, I.; Zhumekenov, A.A.; Begum, R.; Pan, J.; Cho, N.; Mohammed, O.F.; Bakr, O.M. Pure Cs_4PbBr_6: Highly Luminescent Zero-Dimensional Perovskite Solids. *ACS Energy Lett* **2016**, *1*, 840–845, doi:10.1021/acsenergylett.6b00396.
28. Gonzalez-Rodriguez, R.; del Castillo, R.M.; Hathaway, E.; Lin, Y.; Coffer, J.L.; Cui, J. Silicene/Silicene Oxide Nanosheets for Broadband Photodetectors. *ACS Appl Nano Mater* **2022**, *5*, 4325–4335.
29. Zhao, H.; Sun, R.; Wang, Z.; Fu, K.; Hu, X.; Zhang, Y. Zero-Dimensional Perovskite Nanocrystals for Efficient Luminescent Solar Concentrators. *Adv Funct Mater* **2019**, *29*, 1902262, doi:10.1002/adfm.201902262.
30. Benin, B.M.; Dirin, D.N.; Morad, V.; Wörle, M.; Yakunin, S.; Rainò, G.; Nazarenko, O.; Fischer, M.; Infante, I.; Kovalenko, M. V. Highly Emissive Self-Trapped Excitons in Fully Inorganic Zero-Dimensional Tin Halides. *Angewandte Chemie International Edition* **2018**, *57*, 11329–11333, doi:10.1002/anie.201806452.
31. Yin, J.; Zhang, Y.; Bruno, A.; Soci, C.; Bakr, O.M.; Brédas, J.-L.; Mohammed, O.F. Intrinsic Lead Ion Emissions in Zero-Dimensional Cs_4PbBr_6 Nanocrystals. *ACS Energy Lett* **2017**, *2*, 2805–2811, doi:10.1021/acsenergylett.7b01026.
32. Almutlaq, J.; Yin, J.; Mohammed, O.F.; Bakr, O.M. The Benefit and Challenges of Zero-Dimensional Perovskites. *J Phys Chem Lett* **2018**, *9*, 4131–4138, doi:10.1021/acs.jpclett.8b00532.
33. Wen, X.; Zhang, P.; Smith, T.A.; Anthony, R.J.; Kortshagen, U.R.; Yu, P.; Feng, Y.; Shrestha, S.; Coniber, G.; Huang, S. Tunability Limit of Photoluminescence in Colloidal Silicon Nanocrystals. *Sci Rep* **2015**, *5*, 12469, doi:10.1038/srep12469.
34. Chen, X.; Lin, X.; Zhou, L.; Sun, X.; Li, R.; Chen, M.; Yang, Y.; Hou, W.; Wu, L.; Cao, W.; et al. Blue Light-Emitting Diodes Based on Colloidal Quantum Dots with Reduced Surface-Bulk Coupling. *Nat Commun* **2023**, *14*, 284, doi:10.1038/s41467-023-35954-x.
35. Li, Y.; Shao, W.; Chen, L.; Wang, J.; Nie, J.; Zhang, H.; Zhang, S.; Gao, R.; Ouyang, X.; Ouyang, X.; et al. Lead-Halide Cs4PbBr6 Single Crystals for High-Sensitivity Radiation Detection. *NPG Asia Mater* **2021**, *13*, 40, doi:10.1038/s41427-021-00308-w.